Resistance of museum artefacts against blast loading

Filippo Masi, Ioannis Stefanou, Paolo Vannucci, Victor Maffi-Berthier

Resistance of museum artefacts against blast loading

Filippo Masi[a,b,*], Ioannis Stefanou[a], Paolo Vannucci[c], Victor Maffi-Berthier[b]

[a] *Laboratoire Navier, UMR 8205, École des Ponts, IFSTTAR, CNRS, UPE, 6-8 avenue Blaise Pascal, F-77455, Champs-sur-Marne, France.*

[b] *Ingérop Conseil et Ingénierie, 18 rue des Deux Gares, F-92500, Rueil-Malmaison, France.*

[c] *LMV, UMR 8100, Université de Versailles et Saint-Quentin, 55 avenue de Paris, F-78035, Versailles, France.*

Abstract

The response of museum artefacts and statues subjected to deliberate explosions of moderate intensity is investigated and their vulnerability assessed. The study focuses on the most predominant failure mechanisms, namely overturning and fracture due to the tensile stresses developed by the impact of shock waves.

The rocking response is investigated relying on the existing knowledge and theory of inverted pendulum structures subjected to earthquake loadings. An analytical, established approach for determining the overturning domain, developed in a previous study, is used to investigate the critical stand-off distance between the target and the explosive in order to avoid toppling.

The proposed analytical model is adopted by defining appropriate correction parameters to consider the real geometry of the museum objects. We assess the overturning domain of some emblematic statues of high aesthetic and cultural value, and namely: Michelangelo's *David*, *Farnese Hercules*, *Aphrodite of Milos*, *Athena Giustiniani*, *Laocoön and His Sons*, and *Belvedere Torso*.

Finally, direct damage due to the high tensile stresses is investigated and computed for different target geometries. For the dimensions and explosive quantities herein considered, overturning is found to prevail over direct material damage for targets with regular geometry.

Keywords: Museum artefacts; Rocking; Fracture; Blast load; Heritage; Preservation.

1. Research aim

The resistance of un-anchored museum artefacts against fast-dynamic excitations arising from explosions is studied herein. Namely, we investigate the vulnerability of museum artefacts with the aim of providing criteria for their preservation against deliberate blasts of moderate intensity. Two are the main failure mechanisms considered in this study: overturning, produced by the rocking of the artefact, and (direct) material damage caused by the shock waves. We aim at the preservation of un-anchored equipment and museum (slender) artefacts, such as statues. In particular, our study proposes to estimate safety perimeters (passive protections) around such statues for assuring their integrity against explosive's amounts difficult to be identified at the museum's entrance. That is why we consider here moderate intensity blasts.

2. Introduction

The rocking and overturning of artefacts is investigated using the well-established model of the inverted pendulum structures [1, 2, 3, 4, 5]. An analytical approach to compute the rocking response and the overturning domain of slender, rectangular blocks, formerly developed by the authors [6], is here adopted. In particular, moment balance equations and overturning conditions are used to determine the critical (minimum) stand-off distance between the source and the target to prevent toppling.

Besides overturning, direct material damage due to the development of important tensile stresses arising from the impinging blast waves plays a crucial role. Direct material damage is investigated using a detailed Finite Element (FE) simulations.

For the dimensions and explosive quantities considered herein, overturning is found to be predominant for targets with regular geometry. This holds true when considering the strain rate effects (due to the fast-dynamic excitations involved in explosions) and their influence on the material strength (see e.g. [7, 8]). For targets with complex shapes, failure due to direct damage is found to be the predominant mechanism. Sliding and

*Corresponding author.
Email addresses: filippo.masi@enpc.fr (Filippo Masi), ioannis.stefanou@enpc.fr (Ioannis Stefanou), paolo.vannucci@uvsq.fr (Paolo Vannucci), victor.maffi-berthier@ingerop.com (Victor Maffi-Berthier)

uplifting failure modes are always negligible over toppling and material damage.

Engineering applications of the present study can be found in several domains. Of interest here is the preservation of un-anchored equipment and museum (slender) artefacts, such as statues. In particular, we consider some of the most emblematic statues of the world cultural heritage and namely: Michelangelo's *David* (Gallery of the Academy of Florence, Florence), *Farnese Hercules* (Archaeological National Museum, Naples), *Aphrodite of Milos* (Louvre Museum, Paris), *Athena Giustiniani*, *Laocoön and His Sons*, and *Belvedere Torso* (Vatican Museums, Vatican City). These objects belong to the world cultural heritage and their protection has raised important issues throughout history. We refer e.g. to the lost and/or destroyed artefacts of *Athena Parthenos*, *Colossus of Rhodes*, the statue of *Zeus at Olympia*, and more recently the *Buddhas statue* of Bamiyan. The proposed analytical model can further be used in the engineering design framework, for securing historical buildings made of monolithic columns from collapse (e.g. classical Greek and Roman temples [9, 10]).

Diagnostic analyses (to detect the presence of cracks and evaluate the material degradation) as well as 3D technologies for digital survey of the real geometry of the artefacts are mandatory to properly asses their vulnerability, see [11, 12, 13, 14].

Prevention based on active protective devices, e.g. screening, at the entrance of museums may contrast the explosive threat and reduce the risk of damaged artefacts. Nevertheless, we find a strong vulnerability of some existing museum objects, even for small explosive quantities, whose detection may be demanding. Our study proposes to estimate safety perimeters (passive protections) around such statues for assuring their integrity against explosive's amounts difficult to be identified at the museum's entrance. That is why we consider here moderate intensity blasts.

The paper is structured as follows. In Section 3.1 we present the approaches followed to represent blast actions relying on either simplified models or more detailed ones. Section 3.2 focuses on the overturning response mechanism of rectangular, slender blocks

subjected to an explosion. We present an analytical approach, formerly developed by the authors [6], to be used as a straightforward engineering tool to derive the critical stand-off distance between the target and the explosive source to avoid toppling. In Section 3.3, the analytical model is applied to museum artefacts and some emblematic examples of existing statues are presented. Section 3.4 focuses on the vulnerability to direct material damage due to blast loads for rectangular, slender blocks. Finally, in Section 4 the statue of *Aphrodite of Milos* is used to compute the critical stand-off distance to avoid direct material damage, which is compared to the one required to avoid overturning.

3. Material and methods

3.1. Blast actions

Explosion produces a blast wave of high-pressure accompanying high-temperature and supersonic expansion of gases. The abrupt increase of the pressure carried by a blast wave can produce severe structural damage. When the primary shock meets a target, it generates on it the so-called *reflected overpressure*, P_r, which is the difference between the pressure determined by the explosion increased by the reflection at target's surface and the ambient one, P_o. Figure 1 shows the schematic time variation of P_r, which is determined by the arrival time of the shock wave, t_A, the overpressure peak, P_{ro}, the positive phase duration, t_o, negative phase duration, t_{o-}, and the underpressure peak, P_{ro-}. These parameters are functions of the distance R and the explosive weight (conventionally expressed in TNT, trinitrotoluene, equivalent). Herein we consider only the positive phase of the blast wave (safety approach, see [6]).

The pressure acting on a target due to blast loading is the sum of the incident overpressure P_s and the dynamic pressure $C_D\, q := \frac{1}{2}\rho u|u|$, with C_D the drag coefficient (function of the target shape and Mach and Reynold numbers, among other parameters), ρ the density, and u the velocity of gas particles. Notice that the dynamic pressure contribution to the reflected overpressure P_r varies with respect to the stand-off distance: for near-field explosions, the dynamic pressure contribute may be as high as two times the incident pressure (i.e. $q/P_s \approx 2$), while for far-field blasts we record $q/P_s \approx 0.4$, see [15].

The simulation of a blast can be conducted by using different approaches [16, 17], i.e., empirical or physics-based ones. These models are briefly introduced below.

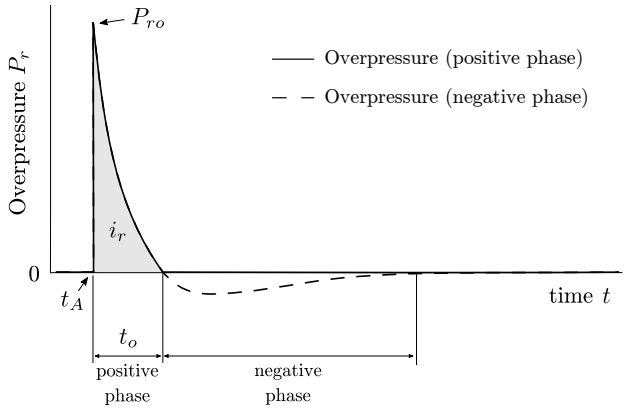

Figure 1: Time evolution of overpressure (i.e. the pressure measured relatively to the atmospheric one) due to an explosion acting on a target. The proposed analytical model only considers the positive phase of the overpressure (safe estimate of the rocking response). The negative pressure may have stabilising effects (increase the block resistance to overturning).

3.1.1. Empirical models

Empirical models rely on best-fit interpolations of experimental results and mainly on those of Kingery and Bulmash [18], which allow to determine the blast parameters and pressure loading from the knowledge of the TNT equivalent explosive weight, W, and the Hopkinson-Cranz scaled distance, $Z = R/\sqrt[3]{W}$ (see Appendix A). The time evolution of the positive phase of the reflected pressure is modelled with the well established *modified Friedlander equation* [19],

$$P_r(t) = P_{ro}\left[\left(1-\frac{t}{t_o}\right)\left(1-\mathscr{H}[t-t_o]\right)\right]\exp\left(-d\frac{t}{t_o}\right), \tag{1}$$

where $\mathscr{H}[\cdot]$ denotes the Heaviside (step) function, d is the exponential decay coefficient, and t_A is taken as the origin of the time axis. The impulse i_r associated to the positive phase, which represents the area beneath the pressure curve, reads

$$i_r = \int_0^{t_o} P_r\, dt = \left[e^{-d}+d-1\right]\frac{P_{ro}\, t_o}{d^2}, \tag{2}$$

The above equation allows to determine the exponential decay coefficient, d, by equating it with the best-fit interpolation of i_r from experiments (see Appendix A).

3.1.2. Numerical physics-based models

Physics-based, numerical approaches allow a rather detailed description of the main features of the blast phenomenon with, of course, an increased calculation cost. They rely on the definition of three domains: the target (statue), the explosive charge, and the surrounding air. Through numerical simulations, detonation, propagation of shock waves and their interaction with deformable structures can be efficiently modelled with a Coupled Eulerian-Langrangian (CEL) scheme. The explosive and air domains are both discretized by Finite Elements (Eulerian description). A Fluid-Structure Interaction (FSI) approach based on a penalty contact algorithm [20] allows to transfer the pressure from the propagating media to the target (Lagrangian description). We model air as a viscous fluid; this is not dictated solely by physical, but also by practical reasons, namely to avoid to avoid numerical, spurious oscillations in the rise in pressure over the blast wave. For a more detailed description of the fluid-structure interaction phenomena and their modelling, we refer to [21, 22, 23, 20]. Further details can also be found in [6].

3.2. Overturning of rectangular, slender blocks

3.2.1. Statement of the problem

The problem of a rigid block resting on a horizontal plane is studied based on the following assumptions (Fig. 2):

i. A rectangular slender, rigid block is assumed with a uniformly distributed mass m. The dimensions of the block are $2b \times 2h \times 2w$ and the radial distance from the rocking pivot point O to the centre of gravity is $r = b \sec \alpha$, where α is the slenderness angle.

ii. The contact with the horizontal plane is assumed punctual at point O (no contact moment). Contact is considered to be unilateral. The angle of friction, φ, is assumed to be sufficiently large to prevent sliding.

iii. The pressure load due to the explosion is exclusively applied on the front surface S (incident surface, see Fig. 2) and the blast wave is assumed to impinge all points of S at the same time (simultaneously) and with the same magnitude (uniformly). We consider the resulting load to act always horizontally and at the block's centroid

as the loading pulse duration is extremely short (i.e., small inclination angle within the duration of the loading). Drag and diffraction phenomena are neglected. The effects of induced ground shocks [24, 25] and the uplifting pressure acting on the target's base [6] are also omitted. Accordingly, contact detonations and near-field explosions are not considered in our model.

These simplifying assumptions are helpful for reducing the complexity of the problem and deriving analytical, closed-form solutions. A corroboration of the adequacy of such model is discussed in Appendix B and an exhaustive discussion and validation can be found in [6]. In particular, it is shown that the minimum distance that has to be assured between the explosive source and the target, such that toppling is avoided, is in good agreement and on the safety side with the one determined by the full and detailed numerical model.

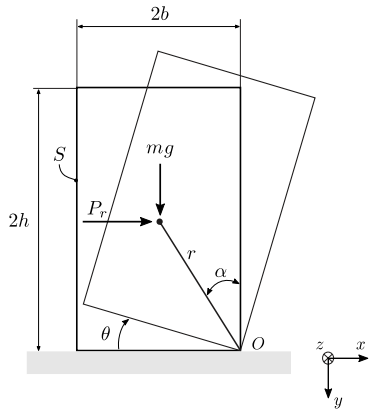

Figure 2: Configuration considered for the rocking problem: a rectangular slender, rigid block resting on a horizontal plane with uniformly distributed mass, subjected to uniform pressure load due to an explosion.

3.2.2. Equation of motion

The moment balance around the rocking pivot point gives the equation of motion

$$\left.\begin{aligned} \mathscr{I}_o\ddot{\theta} + mgr\sin(\alpha-\theta) &= SrP_r\cos(\alpha-\theta), \qquad \theta(t)>0, \\ \mathscr{I}_o\ddot{\theta} + mgr\sin(-\alpha-\theta) &= SrP_r\cos(-\alpha-\theta), \quad \theta(t)<0, \end{aligned}\right\} \tag{3}$$

where $\mathscr{I}_o = (4/3)mr^2$ is the moment of inertia with respect to the pivot point, $\theta = \theta(t)$ is the inclination angle, and $P_r = P_r(t)$ is the loading which is given by the Friedlander

equation (1) as mentioned above.

For tall, slender blocks, angles θ and α are small and the equation of motion (3) can be linearised using the first-order approximations $\sin(\cdot) \cong \cdot$ and $\cos(\cdot) \cong 1$. Furthermore, as we are interested in overturning, we restrict the above equation to positive angles θ, considering a unilateral response mechanism. The blast load duration is indeed at least two orders of magnitude smaller than the characteristic time of the response. For further details, we refer to [6].

Considering the normalized rocking angle $\phi = \theta/\alpha$, Equation (3) reads

$$\ddot{\phi} = \phi + \chi\, p - 1, \tag{4}$$

where $\chi = \frac{1}{2\rho b g}\frac{P_{ro}}{\alpha}$ is the dimensionless rocking moment, i.e., the ratio between the moment due to the blast load and the restoring moment due to gravity;
$p = \left[\left(1 - \frac{\tau}{\tau_o}\right)\left(1 - \mathscr{H}[\tau - \tau_o]\right)\right] e^{-d\frac{\tau}{\tau_o}}$ the normalized Friedlander time-history; and τ_o the ratio between the characteristic time of the load and the time parameter, $T = \sqrt{\frac{\mathscr{I}_o}{mgr}}$, related to the response of the rigid block. Equation (4) admits a closed-form solution, whose expression can be found in [6].

3.2.3. Overturning and critical stand-off distance

For unilateral excitations, overturning happens when the rocking angle $\theta \geq \alpha$ or, equivalently, when $\phi \geq 1$. The overturning condition can be found by equating the total work done by the blast load to the difference in potential energy between positions $\theta = \alpha$ and $\theta = 0$ (see also Housner, [1]):

$$\int_0^\infty rSP_r\, \dot{\theta} \cos\left(\alpha - \theta\right)\, dt \geq mgr(1 - \cos\alpha). \tag{5}$$

Noticing that $P_r\,(t \geq t_o) = 0$ and rearranging the inequality in terms of the normalized rocking angle and dimensionless time, one obtains

$$\alpha r S P_{ro} \int_0^{\tau_o} p\dot{\phi} \cos\left[\alpha(1 - \phi)\right]\, d\tau \geq mgr(1 - \cos\alpha). \tag{6}$$

For the special case of slender blocks, the power series expansion at the first order of $(1 - \cos\alpha) \cong \alpha^2/2$ and $\cos[\alpha(1 - \phi)] \cong 1$, Eq. (6) becomes

$$2I\chi \geq 1, \tag{7}$$

with $I = \int_0^{\tau_o} p\,\dot{\phi}\ d\tau$. The left-hand side term in inequality (7) represents the non-dimensional overturning moment.

From the overturning condition ($2I\chi = 1$) we can determine the minimum required distance between the explosive source and the target, R^*, in order to avoid toppling. Figure 3 shows the contours of the critical distance R^* for different slenderness angles, block heights, densities, and explosive quantities.

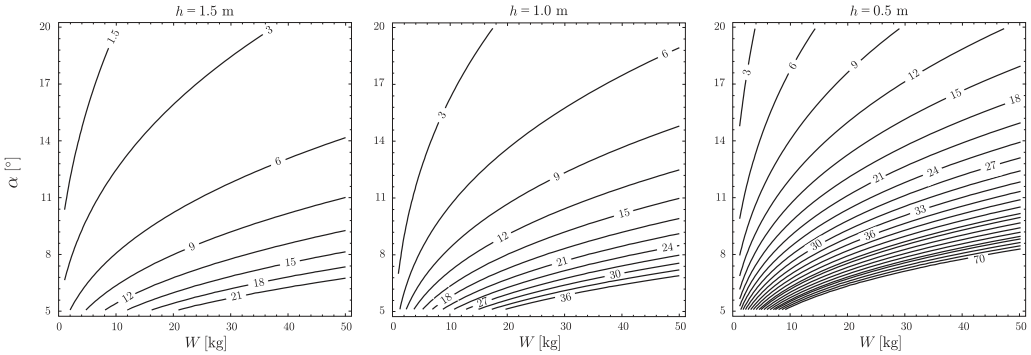

Figure 3: Contours of the critical stand-off distance, i.e., the minimum required distance between the explosive source and the rigid target, R^*, in order to avoid toppling. For $\rho = 2000$ kg/m^3 and heights $h = 1.5$ m (left), $h = 1.0$ m (centre), and $h = 0.5$ m (right), R^* is plotted as a function of the explosive quantity, W, and slenderness, α.

3.3. Overturning of museum artefacts

In this section we consider the overturning of museum objects due to blast loading. A simplified model, described hereafter, is adopted.

The artefact is modelled as a rigid block, with front surface S equal to the front surface of the artefact and moment of inertia around the pivot point O equal to the one of the artefact, $\mathscr{I}_o^\sharp$. With reference to Figure 4, the centre of gravity is located at distance r from the pivot point, at a height $h_g = r\cos\alpha$ from the ground and horizontal distance $b = r\sin\alpha$. The centroid of the front surface, impinged by the blast wave (simultaneously and uniformly), is at height h_c from the ground (see Fig. 4).

Blast loads are modelled as in Section 3.2 (cf. paragraph 3.2.1, (*iii*)). The drag coefficient C_D is supposed to be equal to 2 (C_D of a rectangular target, with surface's normal parallel to direction of the shock front) for front surfaces of any shape. We use the empirical predictions of P_{ro} (Appendix A), which are valid for rectangular objects. This assumption is on the safety side. For instance, a human body-like shaped target has a drag coefficient $C_D \approx 0.97 - 1.43$ [26]. Clearing and lift effects are not considered and they may influence the strength against overturning of museum artefacts of various shapes. Nevertheless, the simplified analytical approach allows for a rapid estimation of the "real" overturning domain. The influence of all the above simplifying assumptions is discussed further in the paper, once the failure due to direct damage has also been presented.

Assuming small slenderness angles α and a unilateral rocking response, the dimensionless equation of motion (4) holds. The dimensionless rocking moment and normalized time are corrected to consider the real geometry of the artefact as follows

$$\chi \to \chi\,(1+\delta)\,, \tag{8}$$

$$\tau \to \frac{\tau}{\sqrt{\kappa}}\,, \tag{9}$$

$$\tau_o \to \frac{\tau_o}{\sqrt{\kappa}}\,, \tag{10}$$

$$\text{with} \quad \kappa = \frac{\mathscr{I}_o^\sharp}{\mathscr{I}_o}, \quad \delta = \frac{h_c - h_g}{r} \tag{11}$$

where κ is the ratio of the moment of inertia of the artefact $\mathscr{I}_o^\sharp$ and of the rectangular block $\mathscr{I}_o$ and δ is the dimensionless contribution to the rocking moment due to the misalignment of the surface centroid and the centre of gravity.

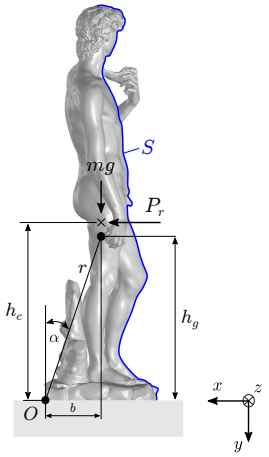

Figure 4: Configuration considered for the rocking problem of museum artefacts: an arbitrarily shaped rigid block with rectangular base, resting on a horizontal plane with uniformly distributed mass (centre of gravity at h_g), subjected to a uniform blast pressure applied to surface S (blue), with centroid at h_c). The arrival of the blast wave at surface S is assumed to be same for each point.

Accordingly, the linearised overturning condition (7) remains the same, $2\chi I \geq 1$. The above mentioned inequality allows to compute the minimum stand-off distance R^*, between a given artefact and a selected explosive quantity, to avoid overturning.

We consider herein some emblematic museum statues belonging to the world cultural heritage as case studies for the assessment of protective barriers, see Figure 5. For each statue, we consider the worst case scenario: a blast wave with a direction such that the statue rocking resistance is the smallest one.

Table 3 shows the overturning domain for each artefact as function of the explosive weight, W. The case of Michelangelo's *David* is particularly interesting. A large height and a high slenderness angle confer to the statue an excellent resistance to rocking, hence to overturning. This is due to a scale effect; as first noticed by Housner [1], at equal slenderness α, the larger the value of r is, the more stable against overturning the block is. Notice that the protective barrier around the statue of Michelangelo's *David* at the Gallery of the Academy of Florence is such that it is impossible to approach the statue closer than ≈ 1.50 m, meaning that the artefact is safe with respect to overturning, for explosive weights as high as 30 kg and greater. The same holds for the statues of

Farnese Hercules and *Aphrodite of Milos*. Diversely, the other statues do not fulfil the standards of a safe design to prevent overturning under explosive loads. For instance, *Laocoön and His Sons* does not have any protective barrier and this might cause its loss for explosive weights as small as 10 kg.

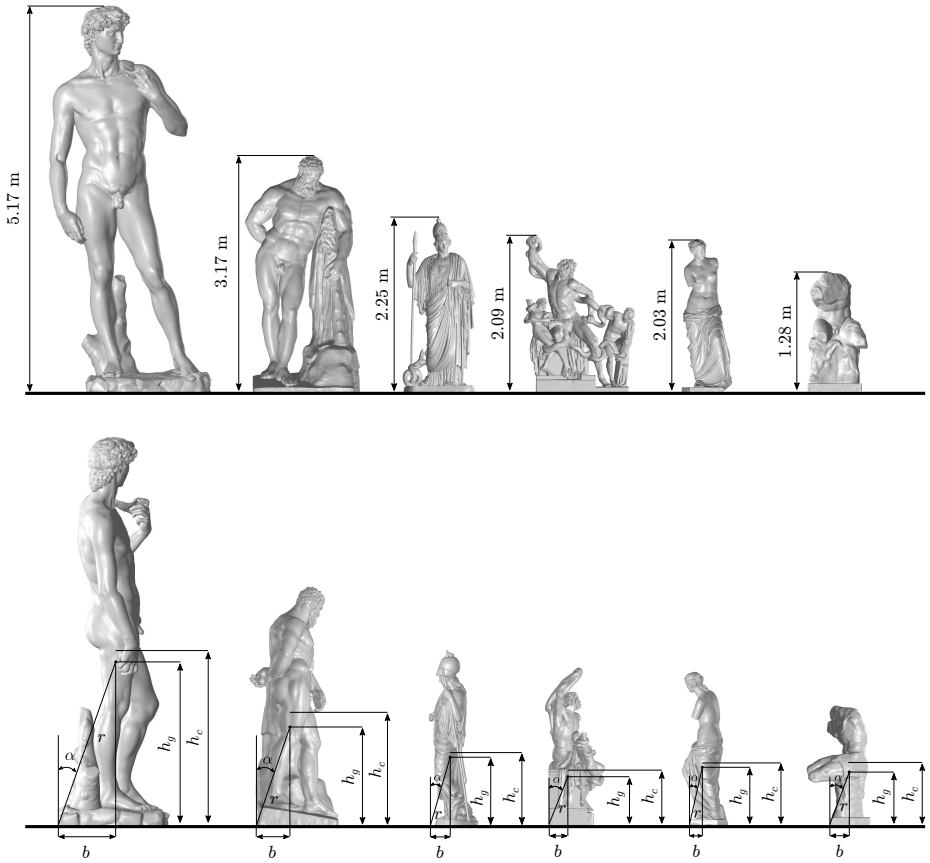

Figure 5: Different museum artefacts considered. From left to right: Michelangelo's *David* (Gallery of the Academy of Florence, Florence), *Farnese Hercules* (Archaeological National Museum, Naples), *Athena Giustiniani* (Vatican Museums, Vatican City), *Laocoön and His Sons* (Vatican Museums, Vatican City), *Aphrodite of Milos* (Louvre Museum, Paris), and *Belvedere Torso* (Vatican Museums, Vatican City). The three-dimensional models are recovered from the platform Scan The World [27].

Table 1: Rocking and overturning parameters for the considered artefacts, recovered from the platform Scan The World [27].

Museum artefact	m [kg]	$\mathscr{I}_o^\sharp$ [kg m^2 $\times 10^3$]	h_g [m]	h_c [m]	α [°]	b [m]	S [m^2]
Michelangelo's David	5800	1650	2.28	2.35	17.6	0.70	5.02
Farnese Hercules	4380	390	1.26	1.41	19.3	0.44	3.39
Athena Giustiniani	765	26.7	0.91	0.92	13.8	0.22	1.39
Laocoön and His Sons	1328	13.6	0.61	0.79	27.1	0.32	1.83
Aphrodite of Milos	565	16.4	0.86	0.87	18.4	0.28	0.83
Belvedere Torso	760	16.5	0.67	0.8	18.7	0.23	0.84

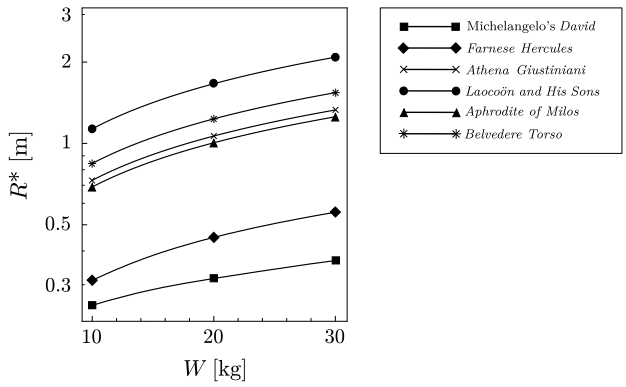

Figure 6: Critical stand-off distance R^* for the considered museum artefacts, as function of the explosive weight W.

3.4. Damage of rectangular, slender blocks

We consider now the conditions that can lead to a (direct) material failure of a museum object under moderate intensity blasts (see Sect. 2). For this study, FE simulations are used to investigate whether or not the development of tensile stresses during the shock waves impact may damage the target. It is rather well known that the tensile strength of geomaterials under high strain rates can be higher than in quasi-static conditions [7]. The same holds for marble [8]. Let us consider the following simplified case. A target, with infinite height (no rocking response mechanism) and square cross-section $A = 0.5 \times 0.5$ m^2, is subjected to an explosion with $R = 1$ m and $W = 10$ kg. To this purpose, a Finite Element model is used assuming the material behaviour as linearly elastic, with Young modulus $E = 40$ GPa and Poisson's ratio $\nu = 0.15$. The pressure load is computed using the empirical interpolations from [18] and applied using ConWep model [28], accounting for the effects due the relative inclination of the impinged surface (locally) with respect to the shock front direction, the non-simultaneity and non-uniformity of the blast pressure for all the impinged surface (and not only on the front face).
Figure 7 presents the normalized stress $\varsigma = \sigma_t / P_{ro}$, with σ_t the maximum principal stress and P_{ro} the overpressure peak. At time $t = 0\,\mu$s, the shock wave impinges the front surface (bottom boundary of section A). A compression wave propagates through the material, with amplitude approximately equal to the overpressure peak, P_{ro}, (cf. [29]). Due to refraction phenomena at the free boundaries, tensile waves generate and interact causing high fluctuations of stress and strain [29, 30, 31]. The further localisation of stress waves results in tensile stresses higher in value than the initial compression stress (see Fig. 7: for $t > 170\,\mu$s, $\varsigma > 1$). The high loading rate of the blast wave gives rise to volumetric (tensile) strain rates as high as 500 s^{-1}.

Extensive experimental research showed that the loading rate influences the resistance of brittle materials mainly due to the finite growth rate of micro-cracks [32, 33] and the viscosity of the material [34]. At increasing strain rates, an increase of the tensile, f_t, and compressive strengths, among other parameters, is observed [7, 35, 8]. The dynamic increase factor for tensile strength for geomaterials (such as mortar, tuff, granite, etc.) usually varies between 1 and approximately 7 in function of the involved strain rates, $\dot{\varepsilon}$

(see [8]). As far it concerns statues, we refer to marble (Carrara marble), whose tensile strength in quasi-static loading conditions is 6.9 MPa and reaches a value of 50 MPa at $\dot{\varepsilon} = 18\ \mathrm{s}^{-1}$, as experimentally observed in [8].

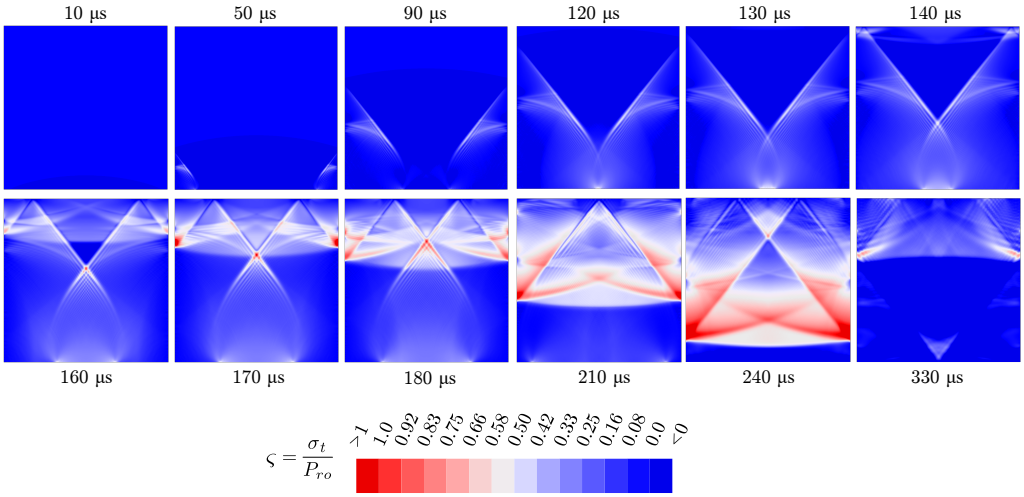

Figure 7: Time evolution of the dimensionless stress $\varsigma = \sigma_t / P_{ro}$ through the cross-section $A = 0.5 \times 0.5$ m^2 of a target due to an explosion ($R = 1$ m, $W = 20$ kg). The time origin is at the shock wave arrival on the free bottom boundary. The initial longitudinal compression wave is refracted at the free boundaries. The tensile release waves interact continuously and cause stress concentrations. The material is assumed to be linear elastic.

In the aforementioned case, strain rates are much higher than 18 s^{-1}. We hence assume a constant tensile strength $f_t = 50$ MPa. The material constitutive law is modified accordingly: in tension, a linear elastic behaviour is assumed until the maximum principal stress reaches the tensile strength. A subsequent tensile softening is considered in terms of the nonlinear brittle cracking model [20, 36, 37]. In compression, the behaviour is assumed to be linearly elastic due to the lower compression stresses involved in the case at hand and the high (strain rate dependent) material strength. This holds true when blast loads of moderate intensity are considered, as in this case. Indeed, at larger blast intensities, material damage may occur due to the large compressive stresses developed at the shock wave impact. The results are displayed in Figure 8.

It worth noticing that, differently from the overturning mechanism, failure due to

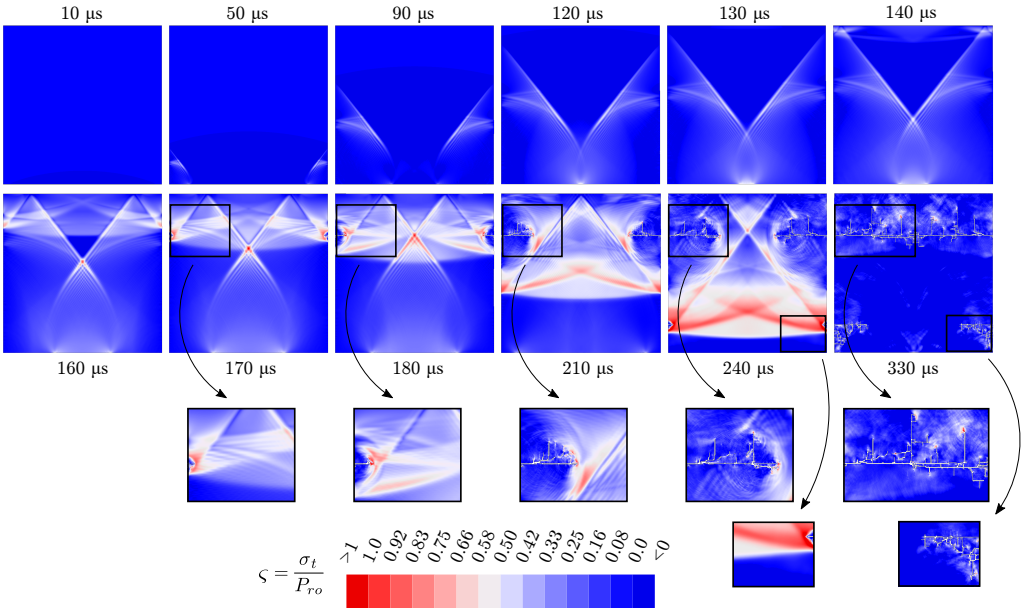

Figure 8: Time evolution of the dimensionless stress $\varsigma = \sigma_t / P_{ro}$ through the cross-section $A = 0.5 \times 0.5$ m^2 of a target due to an explosion ($R = 1$ m, $W = 20$ kg). The time origin is at the shock wave arrival on the free bottom boundary. The initial longitudinal compression wave is refracted at the free boundaries. The tensile release waves interact continuously and cause stress concentrations. Stresses exceeding the material strength results in damage (as shown in zoomed views).

direct damage is not influenced by the local value of the blast pressure acting on the target's surfaces, but rather by the interaction of tensile and compressive waves propagating within the solid material (e.g. marble). Indeed, clearing, drag, lift effects, as well as other complex FSI phenomena have a characteristic time which is two-three orders of magnitude larger than the material response. In other words, failure due to damage takes place in a shorter time with respect to fluid-dynamics phenomena. Indeed, the propagating speed of elastic waves in a solid material may vary between 150 and 200 km/s, in marble, while a shock wave with a Mach number, for instance, equal to $0.5 \div 2.0$ propagates at $170 \div 680$ m/s (in air at atmospheric conditions).

3.4.1. Critical stand-off distance for material failure

The tensile stress, σ_t, originating by refraction phenomena and localisation is, without loss of generality, proportional to the overpressure peak P_{ro}, namely $\sigma_t = \varsigma P_{ro}$. The

focalisation of stress waves may give rise to tensile stresses higher than the blast pressure, i.e., $\varsigma > 1$. In general, the value of ς depends on the material, the geometry of target, the stand-off distance, and the explosive weight.

Damage of a target due to blast loading happens if the tensile stress exceeds the material strength (Galileo-Rankine tension criterion), namely if

$$\frac{\Gamma}{\varsigma} \leq 1 \qquad \text{with} \qquad \Gamma = \frac{f_t}{P_{ro}}. \tag{12}$$

The tensile strength f_t and consequently the dimensionless parameter Γ are functions of the strain rate $\dot{\varepsilon}$.

In the short time period, after the blast wave arrival (see Fig.s 7, 8), this dependency is negligible, due to the high strain rates involved, $\dot{\varepsilon} > 18$ s^{-1}, i.e. $\Gamma = \Gamma_{crit} = \Gamma|_{\dot{\varepsilon} \geq 18 \text{ s}^{-1}}$. Accordingly, Figure 9 displays the values of Γ_{crit} ($\dot{\varepsilon} = 18$ s^{-1}, $f_t = 50$ MPa) for rectangular blocks of several dimensions subjected to different explosive weights. The phenomenon of localisation of tensile stresses gains importance for slender blocks and small cross-sections.

Table 4 compares for each block the critical stand-off distance to avoid material failure, R^*_{dam} , and overturning, R^*. For the dimensions and explosive weights here explored, toppling prevails. In other words, overturning is the most critical failure condition.

This stands only for the relatively short time period following the arrival of the shock wave, when the loading rates are sufficiently high to assume $f_t = 50$ MPa. If a smaller strain rate is assumed *a priori* (and considered constant during the numerical simulations), the corresponding tensile strength decreases and the critical stand-off distance associated to material damage increases. Nevertheless, the dimensionless ratio Γ is only slightly dependent on the strain rate. Consider, for instance, a block with $A = 0.25 \times 0.25$ m^2 subjected to an explosive weight $W = 10$ kg, we obtain the following values

$$\Gamma_{crit} = \Gamma|_{\dot{\varepsilon} \geq 18 \text{ s}^{-1}} = 2.15, \qquad \Gamma|_{\dot{\varepsilon}=1 \text{ s}^{-1}} = 2.02, \qquad \Gamma|_{\dot{\varepsilon} \leq 10^{-4} \text{ s}^{-1}} = 2.40.$$

The corresponding critical stand-off distances to avoid material failure are

$$R^*_{\text{dam}}|_{\dot{\varepsilon} \geq 18 \text{ s}^{-1}} = 1.4 \text{ m} \qquad R^*_{\text{dam}}|_{\dot{\varepsilon}=1 \text{ s}^{-1}} = 2.3 \text{ m}, \qquad R^*_{\text{dam}}|_{\dot{\varepsilon} \leq 10^{-4} \text{ s}^{-1}} = 3.1 \text{ m},$$

while $R^* = 2.27$ m (overturning). Summarizing, blast loads induce two different types of response of a target (prevailing on other ones): rocking (overturning) and damage

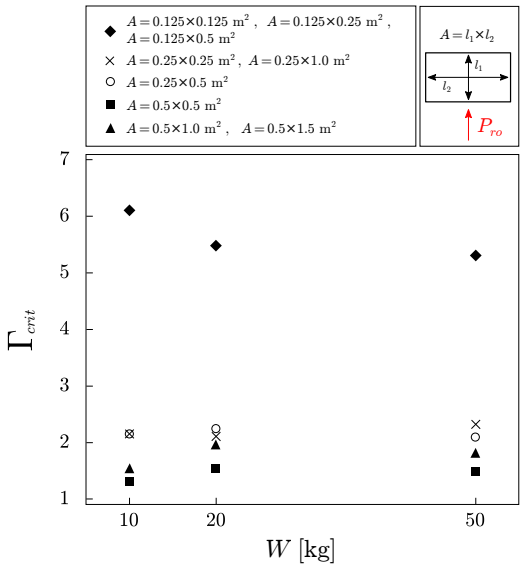

Figure 9: $\Gamma_{crit} = \Gamma|_{\dot{\varepsilon} \geq 18\ \mathrm{s}^{-1}}$, i.e., $f_t = 50$ MPa, as function of the explosive weight for rectangular blocks with height $2h = 2$ m, different cross-sections $A = l_1 \times l_2$ and width $2b = l_1$.

due to tensile stresses. For the case of simple rectangular blocks, overturning is usually predominant. We stress that, however, it is not possible to derive analytical expressions for the material failure condition, as the response is function of the particular geometry of the target and the highly non-linear material behaviour at varying of the strain rate. Each case requires *ad-hoc* investigations to assess the vulnerability to damage. We present an explicative example below.

4. Results and discussion

We focus attention herein on the vulnerability of the statue of *Aphrodite of Milos* against explosive threats. The material behaviour is modelled as described in the previous paragraph and contact at the interface between the statue and the base is considered as in paragraph 5.1. We present in Figure 10 a detail of the geometry and of the numerical model used, consisting of 4-node linear tetrahedra elements of $0.7 \times 0.7 \times 0.7$ cm^3 size (≈ 5.2 millions of FE). ConWep model is used to apply the blast load on all exposed surfaces of the statue (front, rear, lateral sides, and top). We stress that such

Table 2: Comparison of the critical stand-off distance to avoid material failure, R^*_{dam} , and overturning, R^* for blocks of different cross-sections $A = l_1 \times l_2$, width $2b = l_1$, and height $2h = 2$ m. Overturning represents the most critical failure condition.

	$W = 10$ kg		$W = 20$ kg		$W = 50$ kg	
Cross-section A [m^2]	R^*_{dam} [m]	R^* [m]	R^*_{dam} [m]	R^* [m]	R^*_{dam} [m]	R^* [m]
0.125×0.125 0.125×0.25 0.125×0.5	2.15	2.32	2.6	2.92	3.45	3.96
0.25×0.25 0.25×1.0	1.4	2.27	1.75	2.89	2.5	3.95
0.25×0.5	1.4	2.27	1.8	2.89	2.4	3.95
0.5×0.5	1.1	1.76	1.5	2.40	2.05	3.53
0.5×1.0 0.5×1.5	1.56	1.76	1.99	2.40	2.88	3.53

blast load model allows to take into account the inclination of the shock front direction of propagation and the normal to the impinged surface (at a local level, i.e., finite elements), the non-simultaneity ad non-uniformity of the blast pressure over the target's surfaces. Clearing, lift, and drag effects, as well as multiple reflections are neglected, but, as discussed above, their influence is minor when failure due to material damage is under investigation.

Figure 11 displays the time evolution of the dimensionless stress ς due to 10 kg of TNT at a stand-off distance $R = 2$ m. The non-standard geometry of the target gives rise to strong stress localisation. At time $t = 300\,\mu$s after the shock arrival, damage appears in the lower part of the body and propagates within. As the stress waves travel through the material, a strong localisation at the level of the neck takes place and causes its breakage ($t = 950\,\mu$s). Figure 12 displays the damage evolution throughout the body of the statue.

The particular geometry of the statue renders it extremely vulnerable to damage. This is due to the focalisation of the refracted stress waves within the upper part of the

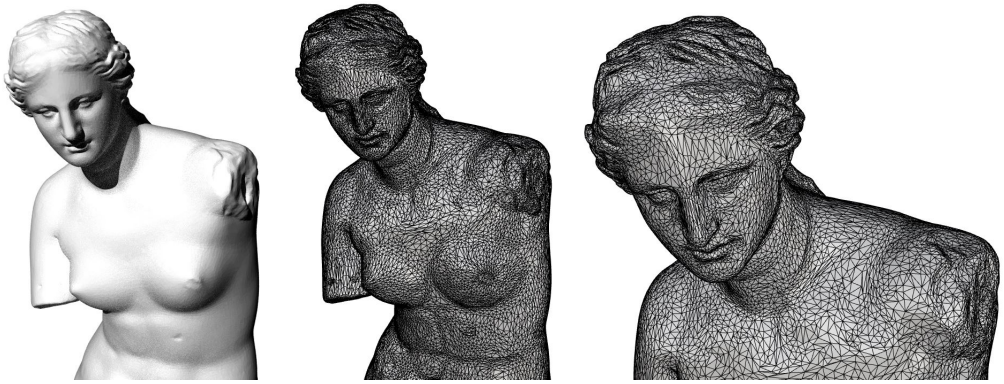

Figure 10: Model used for the statue of *Aphrodite of Milos*.

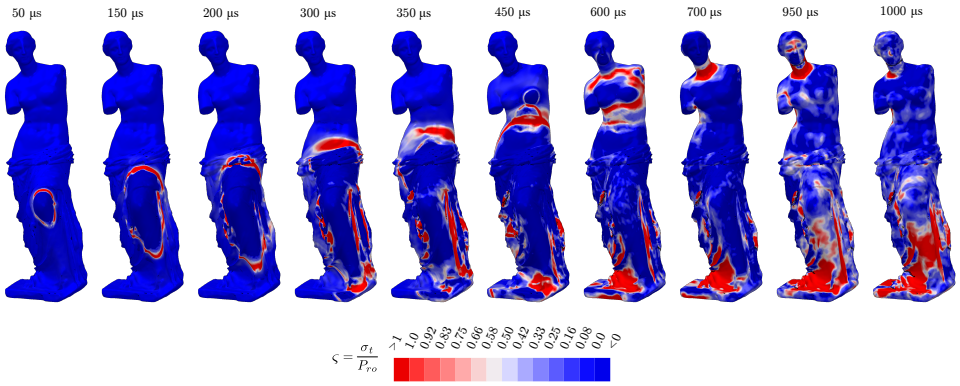

Figure 11: Evolution of the dimensionless stress $\varsigma = \sigma_t / P_{ro}$ due to 10 kg of TNT at a stand-off distance $R = 2$ m from the statue of Aphrodite of Milos.

statue, a phenomenon similar to what observed for blast waves in confined and internal explosions (cf. [22]). Table 5 shows the value of Γ_{crit} to avoid damage of the artefact and compares the critical distances for material failure and overturning. Even if the statue is found to be safe against overturning, the existing protective perimeter around *Aphrodite of Milos*, at Louvre Museum (Paris), is insufficient for the preservation of the artefact against explosions produced by a TNT quantity as great as 10 kg or more.

Moreover, we stress that in the presented analyses we did not consider the eventual material degradation and presence of cracks within the artefact. These features would be responsible to weaken the strength of the statue, e.g. [11]. Hence, for real-case applications, (mechanical) diagnostic analyses and digital surveys are necessary to understand

the *real* strength and the criticality of the failure mechanism.

Table 3: *Aphrodite of Milos* subjected to 10, 20, and 50 kg of TNT. Values of Γ_{crit} to avoid damage of the artefact and comparison between the critical distances for material failure, R^*_{dam}, (critical in this case) and overturning, R^*.

W [kg]	Γ_{crit}	R^*_{dam} [m]	R^* [m]
10	5.87	2.12	0.7
20	5.87	2.67	1.0
50	4.85	3.37	1.66

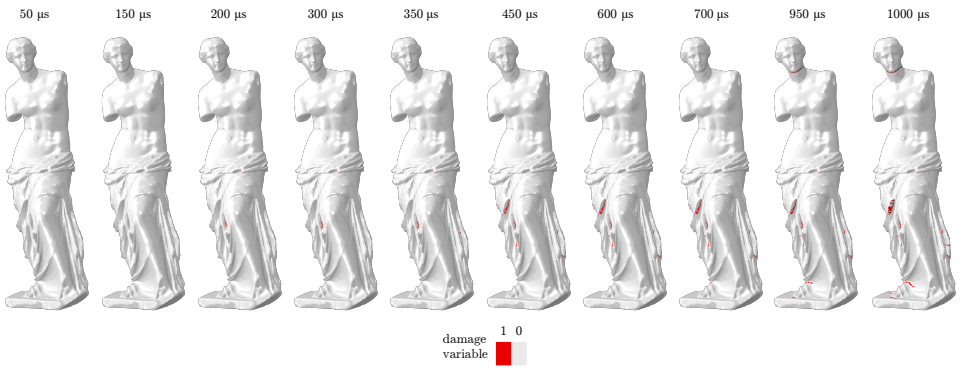

Figure 12: Evolution of damage (i.e., damage when the damage variable is equal to the unit) due to 10 kg of TNT at a stand-off distance $R = 2$ m from the statue of Aphrodite of Milos.

5. Conclusions

We investigated the resistance of museum artefacts under fast-dynamic excitations arising from an explosion. Two main failure mechanisms are considered: failure due to rocking/overturning and failure due to direct material damage.

First, we considered the rocking response mechanism. By virtue of a simplified expression of blast actions based on established empirical models and an analytical approach developed in [6], we presented the overturning condition for rectangular, slender blocks. Attention was focused on the minimum distance (critical stand-off distance) that has to

be assured between the explosive source and the target, such that toppling is avoided. A corroboration of the assumptions of the proposed analytical model was presented in Appendix B with detailed three-dimensional numerical simulations that consider the fluid-structure interaction phenomena, a combined rocking/sliding behaviour, and the possibility of uplifting (flight mode). An exhaustive validation of the analytical approach can be found in [6]. A good agreement was found overall. Moreover, the estimations of the analytical model provide an intrinsic factor of safety (around 2.5) which is consistent for most design applications.

Through the above discussed model, we investigated the vulnerability of some emblematic statues against explosions (by defining appropriate correction factors to consider the actual geometry and mass distribution of artefacts). We assessed the overturning domain of the following statues: Michelangelo's *David*, *Farnese Hercules*, *Athena Giustiniani*, *Laocoön and His Sons*, *Aphrodite of Milos*, and *Belvedere Torso*. We highlighted the criticality of the preservation against explosive threats of some of the artefacts considered. For instance, the statues of *Belvedre Torso*, *Laocoön and His Sons*, and *Athena Giustiniani* were found to be not satisfactorily protected against explosions to prevent overturning.

Finally, direct material damage due to the development of tensile stresses within the body of the targets impinged by the shock wave was investigated. By means of detailed numerical simulations, we found that failure due to overturning prevails on material damage for targets of relatively regular geometry. In other words, the critical stand-off distance to prevent toppling is usually larger than the one to avoid direct material failure. We further investigated the vulnerability to material damage of an existing statue, *Aphrodite of Milos*. In this case, the non-standard geometry of the target gives rise to strong stress concentrations which render the structure more vulnerable to damage rather than overturning.

The purpose of our analysis is to derive reliable decision making tools in the design of protective devices to preserve the historical heritage. We focused attention to the

use of the analytical model for the preservation of museum objects, for determining the minimum perimeter around statues of high historical and aesthetic value. A rather strong vulnerability of such artefacts to explosive threats was found, at least for the considered objects, either due to overturning or direct material damage. Our results can be used to have a first estimation of the protective perimeter to be guaranteed in museums for the investigated statues.

Appendix A. Analytical interpolations for blast loading

The expressions for the blast parameters that determine the reflected pressure time-history due to a surface burst (explosion on or very close to the ground surface) are given below. For more details we refer to [38].

- normal reflected pressure peak P_{ro}:

$$\begin{aligned} P_{ro}(Z) = \left(1 + \frac{1}{2e^{10Z}}\right) \exp\Big[&2.0304 - 1.8036 \ln Z \\ &-0.09293 \ln^2 Z - 0.8779 \sin(\ln Z) - 0.3603 \sin^2(\ln Z)\Big]; \end{aligned} \tag{A.1}$$

- scaled and effective positive reflected impulse i_{rw}, i_r:

$$\begin{aligned} i_{rw}(Z,W) = \exp\Big[&- 0.110157 - 1.40609 \ln Z + 0.0847358 \ln^2 Z\Big], \\ i_r(Z) &= W^{\frac{1}{3}} i_{rw}(Z,W); \end{aligned} \tag{A.2}$$

- scaled and effective arrival time t_{Aw}, t_A:

$$\begin{aligned} t_{Aw}(Z,W) = \exp\Big[&- 0.6847 + 1.4288 \ln Z + 0.0290 \ln^2 Z + 0.4108 \sin(\ln Z)\Big], \\ t_A(Z) &= W^{\frac{1}{3}} t_{Aw}(Z,W); \end{aligned} \tag{A.3}$$

- scaled and effective positive duration time t_{ow}, t_o:

$$\begin{aligned} t_{ow}(Z,W) = \exp\Big[&0.592 + 2.913 \ln Z - 1.287 \ln^2 Z - 1.788 \ln^3 Z \\ &+1.151 \ln^4 Z + 0.325 \ln^5 Z - 0.383 \ln^6 Z \\ &+0.090 \ln^7 Z - 0.004 \ln^8 Z - 0.0004 \ln^9 Z \\ &+0.537 \cos^7\Big[1.032\,(\ln Z - 0.859)\Big] \\ &\sinh\Big[1.088\,(\ln Z - 2.023)\Big]\Big], \\ t_o(Z) = W^{\frac{1}{3}} &t_{ow}(Z,W). \end{aligned} \tag{A.4}$$

Appendix B. Validation of the overturning domain

Whilst the analytical approach above presented can be used to determine the minimum stand-off distance to prevent toppling, it relies on some simplifying assumptions

(see paragraph 3.2.1), whose validity needs to be corroborated. For the sake of completeness, the validation is here conducted by comparison with detailed numerical simulations. An exhaustive validation of the analytical model can by found in [6], where also existing experimental tests are considered.

5.1. Sliding and uplifting effect

We explore *i*) the effect of the linearisation of the equations of motion (see also paragraph 3.2.3), and *ii*) the possibility of the occurence of combined sliding, rocking, and uplift (flight mode). We consider Coulomb friction at the interface of the block with the rigid base, with an angle of friction equal to $\varphi = 35°$, which is common for many geomaterials (concrete, marble, stone etc.). Blast loadings are applied as in Section 3.2, relying on the best-fit interpolations in Appendix A. ABAQUS commercial software is used for the computations. A *hard* contact formulation is used, i.e., no penetration is allowed at the contact of the rocking block with the base [20]. The rigid base is fixed and the rigid block is free to translate along $y-$ and $x-$axes, rotate around z, hence, uplift is possible, see Figure 2. The results of this comparison are presented in paragraph 5.1.

We investigate the minimum stand-off distance (R^*_{num}) for several combinations of slenderness angles and explosive weights. Table 1 displays the comparison between the threshold range (R^*), derived in paragraph 3.2.3, and the one obtained from the numerical simulations (R^*_{num}).

The numerical analyses show that rocking and sliding happen together. However, for slender structures sliding is limited and rocking prevails. In the worst case studied here ($W = 50$ kg and $\alpha = 20°$) the analytical approximation overestimates the minimum stand-off distance by approximately 9%.

5.2. Fluid-structure interaction effect

We focus on the assumptions concerning the simplifications related to the blast loads and their approximation by empirical models. In particular, we investigate the influence of the interaction between blast waves and the rocking block. The analyses are performed again using ABAQUS software. The same modelling approach is used for the interaction of the block and the base as before. The results of this comparison are presented in

Table B.1: Comparison of the overturning domain between the analytical solution, R^* (and corresponding scaled distance Z^*), and the numerical one, R^*_{num}. The rocking block has $h = 1$ m, $\rho = 2000$ kg/m^3, and variable slenderness angle α. Different weights of TNT, W, are considered. Good agreement is found, being always on the safety side.

		$\alpha = 20°$			$\alpha = 15°$			$\alpha = 10°$		
W	[kg]	10	20	50	10	20	50	10	20	50
R^*	[m]	2.18	3.24	5.51	3.40	5.10	8.78	6.53	9.96	17.51
Z^*	[m kg$^{-1/3}$]	1.0	1.19	1.50	1.58	1.88	2.38	3.03	3.67	4.75
R^*_{num}	[m]	2.0	3.0	5.0	3.16	4.75	8.05	6.15	9.3	16.3
$\frac{R^*}{R^*_{\text{num}}}$		1.09	1.08	1.102	1.077	1.073	1.09	1.053	1.071	1.074

paragraph 5.2.

We account for three-dimensional Fluid-Structure Interactions (FSI) with a CEL approach (cf. [22]): the balloon analogue models the explosive source and air is assumed as an ideal gas. The material parameters for the constitutive laws of the balloon are those detailed in [21] (p. 645, model #6). To ensure mesh convergence, the elements size of the Eulerian domain is fixed to 1.0 cm.

The numerical analyses account for the blast negative phase, drag and lift effects, diffraction and rarefaction phenomena, multiple reflections, no-normal incident angle of the blast waves with all the faces (including the base) of the rocking block, and the three-dimensionality of the shock front. These effects result generally in an overall reduction of the blast impulse with respect to the analytical model.

The detailed numerical analyses showed limited influence of lift and drag effects even for combinations of stand-off distance and explosive weight close to the critical ones.

Table 2 presents the critical distance, as obtained from the numerical simulations. The analytical model provides a safe estimate of the critical stand-off distance (upper bound). We notice that an intrinsic factor of safety greater than 2 (ordinary value in any engineering design) is obtained with respect to the detailed numerical simulations. An additional validation of the proposed model can be found in [6], where the critical stand-off distance and dynamic response predictions are corroborated through existing

experimental tests.

Table B.2: Comparison of the overturning domain between the analytical solution, R^* (and corresponding scaled distance Z^*), and the numerical one, R^*_{FSI}. The rocking block has $h = 1$ m, $\rho = 2000$ kg/m^3, and slenderness angle $\alpha = 15°$. Different weights of TNT, W, are considered. The analytical model gives a factor of safety ≈ 2.5 with respect to the numerical solution.

		$\alpha = 15°$		
W	[kg]	10	20	50
R^*	[m]	3.40	5.10	8.78
Z^*	[m kg$^{-1/3}$]	1.58	1.88	2.38
R^*_{FSI}	[m]	1.50	2.25	3.35
$\frac{R^*}{R^*_{\mathrm{FSI}}}$		2.26	2.26	2.62

References

[1] G. W. Housner, The behavior of inverted pendulum structures during earthquakes, Bulletin of the seismological society of America 53 (2) (1963) 403–417.
URL http://resolver.caltech.edu/CaltechAUTHORS:20140801-112753969

[2] J. Zhang, N. Makris, Rocking response of free-standing blocks under cycloidal pulses, Journal of Engineering Mechanics 127 (5) (2001) 473–483. doi:10.1061/(ASCE)0733-9399(2001)127:5(473).

[3] E. G. Dimitrakopoulos, M. J. DeJong, Revisiting the rocking block: closed-form solutions and similarity laws, Proceedings of the Royal Society of London A: Mathematical, Physical and Engineering Sciences 468 (2144) (2012) 2294–2318. doi:10.1098/rspa.2012.0026.

[4] L. Li, J. Du, H. Liu, R. Chen, T. Liu, Dynamic characteristics and seismic responses of painted sculptures of Dunhuang Mogao Grottoes, Journal of Cultural Heritage 22 (2016) 1040 – 1048. doi:https://doi.org/10.1016/j.culher.2016.07.003.
URL http://www.sciencedirect.com/science/article/pii/S1296207416301315

[5] C. C. Spyrakos, C. A. Maniatakis, I. M. Taflampas, Application of predictive models to assess failure of museum artifacts under seismic loads, Journal of Cultural Heritage 23 (2017) 11 – 21. doi:https://doi.org/10.1016/j.culher.2016.10.001.
URL http://www.sciencedirect.com/science/article/pii/S129620741630259X

[6] F. Masi, I. Stefanou, P. Vannucci, V. Maffi-Berthier, Rocking response of inverted pendulum structures under blast loading, International Journal of Mechanical Sciences 157–158 (2019) 833–848. doi:https://doi.org/10.1016/j.ijmecsci.2019.05.024.

[7] C. A. Ross, J. Tedesco, et al., Split-Hopkinson pressure-bar tests on concrete and mortar in tension and compression, Materials Journal 86 (5) (1989) 475–481. doi:https://doi.org/10.14359/2065.

[8] L. N. Y. Wong, C. Zou, Y. Cheng, Fracturing and failure behavior of carrara marble in quasistatic and dynamic brazilian disc tests, Rock Mechanics and Rock Engineering 47 (4) (2014) 1117–1133. doi:10.1007/s00603-013-0465-9.

[9] I. Stefanou, I. Vardoulakis, A. Mavraganis, Dynamic motion of a conical frustum over a rough horizontal plane, International Journal of Non-Linear Mechanics 46 (1) (2011) 114–124. doi:https://doi.org/10.1016/j.ijnonlinmec.2010.07.008.

[10] Rocking and kinematic approaches for rigid block analysis of masonry walls: State of the art and recent developments, Buildings 7 (4) (2017) 69. doi:10.3390/buildings7030069.

[11] A. Borri, A. Grazini, Diagnostic analysis of the lesions and stability of Michelangelo's David, Journal of Cultural Heritage 7 (4) (2006) 273 – 285. doi:https://doi.org/10.1016/j.culher.2006.06.004.
URL http://www.sciencedirect.com/science/article/pii/S1296207406000768

[12] L. Arbace, E. Sonnino, M. Callieri, M. Dellepiane, M. Fabbri, A. I. Idelson, R. Scopigno, Innovative uses of 3D digital technologies to assist the restoration of a fragmented terracotta statue, Journal of Cultural Heritage 14 (4) (2013) 332 – 345. doi:https://doi.org/10.1016/j.culher.2012.06.008.
URL http://www.sciencedirect.com/science/article/pii/S1296207412001070

[13] M. Bagnéris, F. Cherblanc, P. Bromblet, E. Gattet, L. Gügi, N. Nony, V. Mercurio, A. Pamart,

A complete methodology for the mechanical diagnosis of statue provided by innovative uses of 3D model. Application to the imperial marble statue of Alba-la-Romaine (France), Journal of Cultural Heritage 28 (2017) 109 – 116. doi:https://doi.org/10.1016/j.culher.2017.05.002.
URL http://www.sciencedirect.com/science/article/pii/S1296207417300146

[14] K. Čížová, K. Vizárová, A. Ház, A. Vykydalová, Z. Cibulková, P. Šimon, Study of the degradation of beeswax taken from a real artefact, Journal of Cultural Heritage 37 (2019) 103 – 112. doi:https://doi.org/10.1016/j.culher.2018.04.020.
URL http://www.sciencedirect.com/science/article/pii/S1296207417308774

[15] V. Karlos, G. Solomos, Calculation of blast loads for application to structural components, Tech. rep., Joint Research Center of the European Commission (2013). doi:10.2788/61866.

[16] A. M. Remennikov, A review of methods for predicting bomb blast effects on buildings, Journal of Battlefield Technology 6 (2003) 5–10.

[17] M. Larcher, F. Casadei, Explosions in complex geometries — a comparison of several approaches, International Journal of Protective Structures 1 (2) (2010) 169–195. doi:10.1260/2041-4196.1.2.169.

[18] C. N. Kingery, G. Bulmash, Technical report arbrl-tr-02555: Air blast parameters from tnt spherical air burst and hemispherical burst, Tech. rep., U.S. Army Ballistic Research Laboratory (1984).

[19] F. G. Friedlander, The diffraction of sound pulses. i. diffraction by a semi-infinite plate., Proceedings of the Royal Society of London A (186) (1946) 322 – 344.

[20] ABAQUS, Abaqus analysis user's guide, Tech. Rep. Abaqus 6.14 Documentation, Simulia Corp. (2016).

[21] L. Blanc, S. Santana Herrera, J. L. Hanus, Simulating the blast wave from detonation of a charge using a balloon of compressed air, Shock Waves 28 (4) (2018) 641–652. doi:10.1007/s00193-017-0774-0.

[22] F. Masi, I. Stefanou, P. Vannucci, A study on the effects of an explosion in the Pantheon of Rome, Engineering Structures 164 (2018) 259–273. doi:10.1016/j.engstruct.2018.02.082.

[23] F. Masi, P. M. Mariano, P. Vannucci, Blast actions in aircrafts: An integrated methodology for designing protection devices, Engineering Structures 175 (2018) 895 – 911. doi:https://doi.org/10.1016/j.engstruct.2018.08.082.
URL http://www.sciencedirect.com/science/article/pii/S0141029617336994

[24] H. Hao, Y. Zhou, Dynamic response of rigid blocks to simultaneous horizontal and vertical ground shock, Advances in Structural Engineering 15 (7) (2012) 1069–1082. arXiv:https://doi.org/10.1260/1369-4332.15.7.1069, doi:10.1260/1369-4332.15.7.1069.

[25] K. Scherbatiuk, N. Rattanawangcharoen, Experimental testing and numerical modeling of soil-filled concertainer walls, Engineering Structures 30 (12) (2008) 3545 – 3554. doi:https://doi.org/10.1016/j.engstruct.2008.05.030.

[26] A. D. Penwarden, P. F. Grigg, R. Rayment, Measurements of wind drag on people standing in a wind tunnel, Building and environment 13 (2) (1978) 75–84.

[27] MyMiniFactory, Scan The World, 5 Sycamore Street, London, UK.

URL https://www.myminifactory.com/scantheworld/#home

[28] D. Hyde, Conwep: Conventional weapons effects program, US Army Engineer Waterways Experiment Station, USA 2.

[29] M. A. Meyers, Dynamic behavior of materials, John wiley & sons, 1994. doi:https://doi.org/10.1002/9780470172278.

[30] F. Vales, S. Moravka, R. Brepta, J. Cerv, Wave propagation in a thick cylindrical bar due to longitudinal impact, JSME international journal. Ser. A, Mechanics and material engineering 39 (1) (1996) 60–70.

[31] X. Gu, Q. Zhang, D. Huang, Y. Yv, Wave dispersion analysis and simulation method for concrete shpb test in peridynamics, Engineering Fracture Mechanics 160 (2016) 124 – 137. doi:https://doi.org/10.1016/j.engfracmech.2016.04.005.

[32] L. Freund, Crack propagation in an elastic solid subjected to general loading—I. Constant rate of extension, Journal of the Mechanics and Physics of Solids 20 (3) (1972) 129 – 140. doi:https://doi.org/10.1016/0022-5096(72)90006-3.

[33] L. Freund, Crack propagation in an elastic solid subjected to general loading—II. Non-uniform rate of extension, Journal of the Mechanics and Physics of Solids 20 (3) (1972) 141 – 152. doi:https://doi.org/10.1016/0022-5096(72)90007-5.

[34] J. Weerheijm, Concrete under impact tensile loading and lateral compression, Ph.D. thesis, TU Delft, Delft University of Technology (1992).

[35] S. H. Cho, Y. Ogata, K. Kaneko, Strain-rate dependency of the dynamic tensile strength of rock, International Journal of Rock Mechanics and Mining Sciences 40 (5) (2003) 763 – 777. doi:https://doi.org/10.1016/S1365-1609(03)00072-8.

[36] A. Hillerborg, M. Modéer, P. E. Petersson, Analysis of crack formation and crack growth in concrete by means of fracture mechanics and finite elements, Cement and Concrete Resistance 6 (1976) 773–782.

[37] F. Masi, I. Stefanou, P. Vannucci, On the origin of the cracks in the dome of the Pantheon in Rome, Engineering Failure Analysis 92 (2018) 587 – 596. doi:https://doi.org/10.1016/j.engfailanal.2018.06.013.

[38] P. Vannucci, F. Masi, I. Stefanou, A study on the simulation of blast actions on a monumental structure (2017).
URL https://hal.archives-ouvertes.fr/hal-01447783v3/document